energies

Article

A 5.8 GHz π-Stub Decoupling Network for Receiving Antenna Arrays in Microwave Wireless Power Transmission

Xinyuan Li, Hui Xiao, Huaiqing Zhang, Zhewei Liu and Wenxiong Peng *

School of Electrical Engineering, Chongqing University, Chongqing 400044, China
* Correspondence: pwx@cqu.edu.cn

Abstract: In this paper, a 5.8 GHz π-stub decoupling network is proposed to improve the performance of a receiving antenna array (RAA) in microwave wireless power transmission (MWPT) systems. A set of general design formulas was derived for determining the electric parameters of the required π-stubs. To validate the new technique, a π-stub decoupling network was combined with RAAs. The simulated and measured results show that the performance of the RAA is greatly improved by loading the π-stub decoupling network. In addition, a miniaturized MWPT system was built. System-level measurements indicate that the novel decoupling network enhances the receiving power of the RAA by up to 36.4%. An extended application also shows the scalability and effectiveness of the network, implying its huge potential in large-scale receiving arrays.

Keywords: antenna array; decoupling network; microwave wireless power transmission

Citation: Li, X.; Xiao, H.; Zhang, H.; Liu, Z.; Peng, W. A 5.8 GHz π-Stub Decoupling Network for Receiving Antenna Arrays in Microwave Wireless Power Transmission. *Energies* **2022**, *15*, 8703. https://doi.org/10.3390/en15228703

Academic Editors: Yang Li and Pengcheng Zhang

Received: 27 October 2022
Accepted: 17 November 2022
Published: 19 November 2022

1. Introduction

Since microwave wireless power transmission (MWPT) was proposed in 1968 [1], it has received a lot of attention. The advantages of not requiring a transmission line and having flexibility [2] enable it to be applied in many special conditions, such as multi-target and moving target power supply, isolated island power supply, etc. [3–6]. The receiving antenna array (RAA) plays a crucial role in the MWPT system, and its performance directly determines the overall efficiency. Usually, the microstrip antenna array is widely used as the RAA because of its light weight, small volume, and easy integration. The receiving efficiency of RAAs can be improved by expanding the effective area or increasing the gain [7]. Without significantly enlarging the antenna volume, the increase in the RAA area and gain will further compress the gaps between the elements in the array. In addition, the limited space constraint and the trend of miniaturization also require the element gap to be sufficiently small. Some typical examples of RAAs are shown in Table 1.

When the gap is less than $\lambda/2$, a strong coupling will be generated between the elements, which is harmful to the impedance matching, radiation direction, and gain of the array. So, it is crucial to consider the effect of coupling when designing RAAs. In recent years, various methods have been developed in research on reducing mutual coupling. In [8–10], some electromagnetic bandgap (EBG) structures were presented. However, this kind of structure is not suitable for RAAs because the EBGs themselves occupy too much space. In [11], a defected ground structure (DGS) was proposed. The DGS could introduce a current redistribution to decrease the mutual coupling, but the radiation patterns could deteriorate [12]. In addition, there are neutralization lines [13–15], decoupling metasurfaces [16,17], decoupling networks [18,19], etc. Among these methods, decoupling networks are superior due to their simple structure, the adaptability of their design principles, and their flexible element gaps [20]. However, according to Table 1, most of the present MWPT systems ignore the coupling problem of RAAs. Since they did not address the effect of mutual coupling, the negative effect of mutual coupling on receiving power is unknown.

Table 1. A few typical RAAs in MWPT systems.

Reference	Frequency (GHz)	Size (m)	Spacing	Consideration of Coupling Effects
[2]	5.7~6.3	0.07 × 0.07	<0.36 λ	No
[21]	5.8	1 × 1	0.22 λ	No
[22]	5.8	1.38 × 1.38	0.35 λ	No
[23]	5.8	0.5 × 0.5	0.19 λ	No

This study applied decoupling techniques to RAAs for the first time and proposed a 5.8 GHz π-stub decoupling network for MWPT to improve the receiving power of the RAAs. In Section 2, the design principle and formula of the π-stub decoupling network are presented. Section 3 proposes an antenna array, and the application of the decoupling network to the antenna array is described to verify its decoupling effect. Section 4 presents a miniaturized MWPT experimental system built to compare the difference in receiving power before and after decoupling. Section 5 presents an extended application of the π-stub decoupling network. Finally, conclusions are given in Section 6.

2. Design of the Decoupling Network

Considering that the π-stub decoupling network can provide a wider decoupling bandwidth, it is highly suitable for RAAs [24]. As shown in Figure 1a, the proposed π-stub decoupling network is connected in parallel with the coupled antenna network.

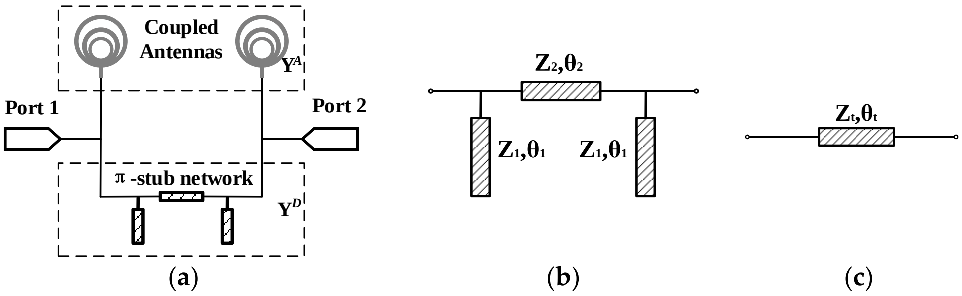

Figure 1. (**a**) Decoupled antenna topology. (**b**) Circuit schematic of the proposed π-stub network. (**c**) The equivalent circuit.

It is assumed that the admittance matrix of the two coupled antennas and the decoupling network are represented by $[Y^A]$ and $[Y^D]$, respectively. Then, the total admittance of the decoupled antennas is the sum of the two matrices, as shown in (1).

$$Y = \begin{bmatrix} Y_{11} & Y_{12} \\ Y_{13} & Y_{14} \end{bmatrix} = \begin{bmatrix} Y_{11}^A + Y_{11}^D & Y_{12}^A + Y_{12}^D \\ Y_{21}^A + Y_{21}^D & Y_{22}^A + Y_{22}^D \end{bmatrix} \tag{1}$$

For an ideal well-matched two-port network, the S-matrix of all elements should be equal to 0, so the normalized Y-matrix after the S-Y transformation is

$$Y = \begin{bmatrix} 1 & 0 \\ 0 & 1 \end{bmatrix} \tag{2}$$

When (1) is equal to (2), antennas can reach high isolation and are well-matched after loading the decoupling network. It is worth noting that $[Y^D]$ is a purely imaginary matrix because the decoupling network is lossless. Set (1) is equal to (2), so then the decoupling conditions can be obtained:

$$j \cdot \mathrm{Im}[Y_{21}^A] + Y_{21}^D = 0 \tag{3}$$

$$\mathrm{Re}[Y_{21}^A] = 0 \tag{4}$$

The matching conditions are:

$$j \cdot \mathrm{Im}[Y_{11}^A] + Y_{11}^D = 0 \tag{5}$$

$$\mathrm{Re}[Y_{11}^A] = 1 \tag{6}$$

where (3) is the decoupling target, and (4) shows no power loss due to coupling when the original coupled antenna is working. Condition (5) requires that the self-admittance of the decoupling network be able to counteract that of the coupled array, and (6) shows that the original coupled antenna is well matched. Since the original antenna is symmetric, only Y_{11} and Y_{21} are considered. In summary, when the decoupling network reaches the requirements of (3)–(6), high isolation can be achieved.

Figure 1b shows the proposed π-stub decoupling network and its equivalent circuit, where Z_1, θ_1, Z_2, and θ_2 are the characteristic impedance and electrical length of the corresponding stubs at 5.8 GHz. The ABCD matrix of the π-stub network is

$$\begin{aligned} \begin{bmatrix} A & jB \\ jC & D \end{bmatrix} &= \begin{bmatrix} 1 & 0 \\ j\frac{\tan\theta_1}{Z_1} & 1 \end{bmatrix} \times \begin{bmatrix} \cos\theta_2 & jZ_2\sin\theta_2 \\ j\frac{\sin\theta_2}{Z_2} & \cos\theta_2 \end{bmatrix} \times \begin{bmatrix} 1 & 0 \\ j\frac{\tan\theta_1}{Z_1} & 1 \end{bmatrix} \\ &= \begin{bmatrix} \cos\theta_2 - \frac{Z_2\sin\theta_2\tan\theta_1}{Z_1} & jZ_2\sin\theta_2 \\ j\left(\frac{2\cos\theta_2\tan\theta_1}{Z_1} + \frac{\sin\theta_2}{Z_2} - \frac{Z_2\sin\theta_2\tan^2\theta_1}{{Z_1}^2}\right) & \cos\theta_2 - \frac{Z_2\sin\theta_2\tan\theta_1}{Z_1} \end{bmatrix} \end{aligned} \tag{7}$$

Comparing the entries of the ABCD matrix with the corresponding entries of the equivalent circuit, the following equations can be obtained.

$$\begin{cases} \cos\theta_2 - \frac{Z_2\sin\theta_2\tan\theta_1}{Z_1} = \cos\theta_t \\ Z_2\sin\theta_2 = Z_t\sin\theta_t \\ \frac{2\cos\theta_2\tan\theta_1}{Z_1} + \frac{\sin\theta_2}{Z_2} - \frac{Z_2\sin\theta_2\tan^2\theta_1}{{Z_1}^2} = \frac{\tan\theta_t}{Z_t} \end{cases} \tag{8}$$

This can be simplified to

$$2\cos\theta_2 \cdot \frac{\cos\theta_2 - \cos\theta_t}{Z_t\sin\theta_t} + \frac{\sin\theta_2}{Z_2} - Z_2\sin\theta_2 \cdot \left(\frac{\cos\theta_2 - \cos\theta_t}{Z_t\sin\theta_t}\right)^2 = \frac{\tan\theta_t}{Z_t} \tag{9}$$

$$\frac{\tan\theta_1}{Z_1} = \frac{\cos\theta_2 - \cos\theta_t}{Z_t\sin\theta_t} \tag{10}$$

Z_t and θ_t are predefined parameters, and Equation (9) contains only Z_2 and θ_2. Hence, θ_1 and θ_2 can be calculated by choosing the appropriate Z_1 and Z_2. According to (10), the π-stub decoupling network can be designed, which has a good match with RAAs.

3. Application to RAAs

3.1. The 1 × 2 RAA

In order to demonstrate the effect of the π-stub decoupling network, a pair of 5.8 GHz RAAs were designed, simulated, and measured. The 1 × 2 RAA resonated at 5.8 GHz and was designed on a polyimide with a thickness of 0.1 mm (ε_r = 3.5, tan σ = 0.002), and a 1 mm air gap was set for better impedance matching. The edge-to-edge distance of the antenna was 6 mm (0.11 λ_0). The antenna geometry and parameters are shown in Figure 2 and Table 2.

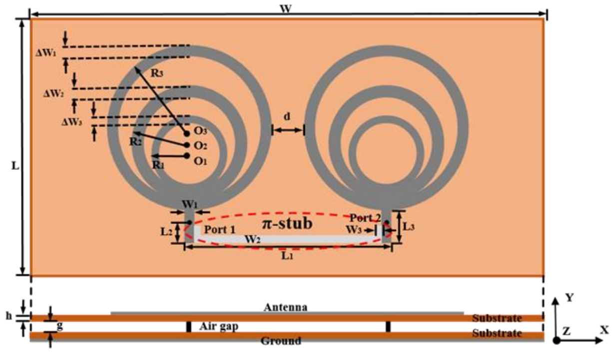

Figure 2. Geometry of the 1 × 2 RAA.

Table 2. Dimensions of the 1 × 2 antenna array shown in Figure 2.

Parameter	Unit: mm	Parameter	Unit: mm	Parameter	Unit: mm	Parameter	Unit: mm
W	90	ΔW_1	1.67	L_1	23.06	R_2	10
W_1	1.4	ΔW_2	1.83	L_2	2.37	R_1	6.5
W_2	1	ΔW_3	0.83	L_3	4.35	g	1
W_3	1	L	45	R_3	14.38	h	0.1

In order to solve the specific parameters of the required π-stub decoupling network, the equivalent circuit needs to be obtained first. It is known that a length of transmission line can act as a phase converter, and once it is added in the proper position, the transmission current can offset the coupling one. Therefore, a meander line can be attached between the two microstrip lines for decoupling purposes. Here, considering that the original array is well matched, conditions (4) and (6) are satisfied, and (5) can be achieved by selecting the proper L_2. Hence, (3) is considered the optimization goal.

Figure 3 shows the relevant Y parameters for (3) and (4). It is clearly seen that at 5.8 GHz, the real part of Y_{21}^{A} is close to 0, and the imaginary part is offset from the imaginary part of Y_{21}^{D}. Therefore, according to the simulation in CST, it can be determined that the meander line can effectively decouple the 1 × 2 RAA at a length of 33.2 mm and a width of 0.41 mm.

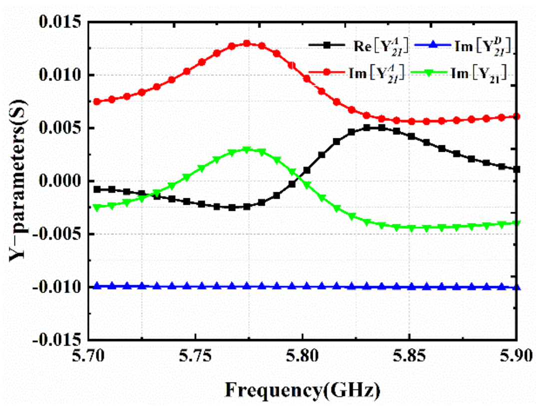

Figure 3. Simulated Y−parameters of (3) and (4).

Thus, the parameters of the equivalent circuit can be determined as Z_t = 172.6 Ω and θ_t = 232.4°. However, the complex structure of the meander line imposes constraints on the element gaps and takes up more space, with little potential for larger arrays. Instead, the simple structure of the π-stub decoupling network is convenient for integration. According to the π-stub design formula and choosing $Z_1 = Z_2$ = 50 Ω, we can obtain θ_1 = 4.97° and θ_2 = 148.87°. The designed decoupling network is shown in Figure 2.

The related simulation results are shown in Figure 4. It can be seen that the original RAA coupling coefficient at 5.8 GHz is −15.1 dB. The mutual coupling decreases by 10.5 dB when the meander line takes effect, while the mutual coupling decreases by 16.7 dB when the π-stub decoupling network is added, and S_{11} decreases from −11 dB to −27 dB.

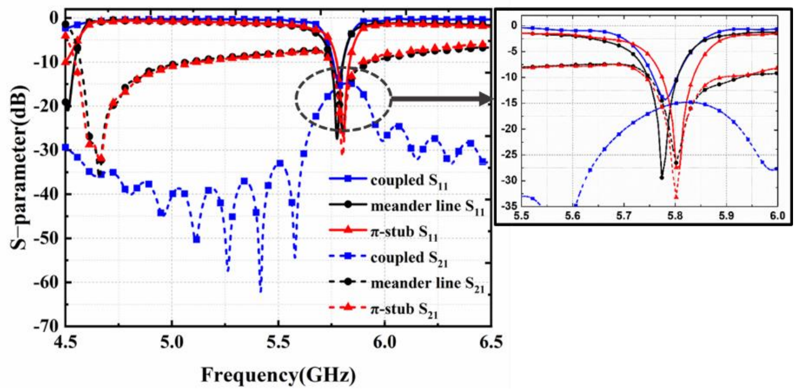

Figure 4. Simulated S−parameters of three 1 × 2 RAAs.

Moreover, the decoupling effect of the π-stub network can be understood by the surface current distribution. When port 1 is excited, the coupled element is strongly influenced, but it is obvious that the coupled current is greatly weakened after loading the π-stub decoupling network, as shown in Figure 5.

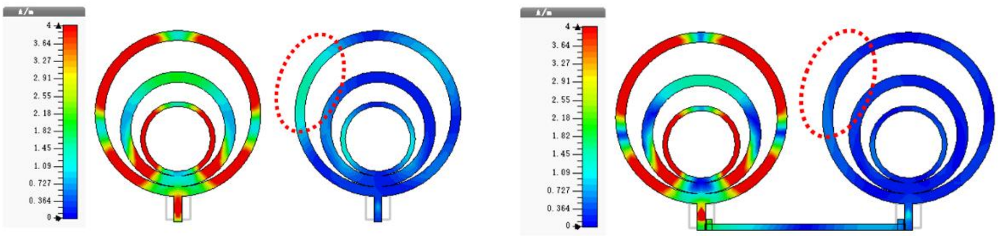

(**a**) (**b**)

Figure 5. Current distribution of the 1 × 2 RAA. (**a**) Without π-stub. (**b**) With π-stub.

To prove the application value, the antennas were fabricated and measured. The prototypes are shown in Figure 6. The air gap is replaced by PMI (Polymethacrylimide, ε_r = 1.02). The S−parameters were measured using an R&S ZVA-50 vector network analyzer, and the results are shown in Figure 7. It can be seen that S_{11} at 5.8 GHz decreases from −12.1 dB to −17.9 dB, achieving a better match. It is evident that due to the π-stub, a 15.3 dB mutual coupling reduction is achieved. The measured and simulated results are in good agreement. In addition, the antenna radiation patterns were measured by using a DONGSHIN ISPACE-6000 microwave anechoic chamber. When port 1 is excited, port 2 is terminated with a matching load. The measurement setup is shown in Figure 8.

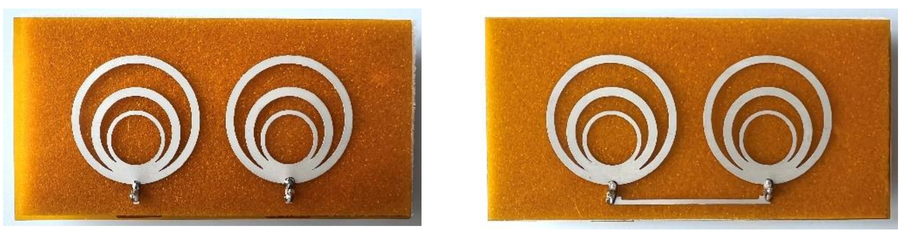

(**a**) (**b**)

Figure 6. The 1 × 2 RAA prototypes. (**a**) Without π-stub. (**b**) With π-stub.

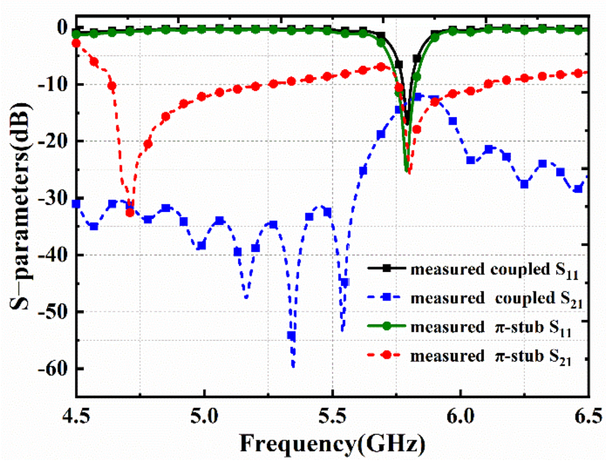

Figure 7. S−parameters of the 1 × 2 RAA prototypes.

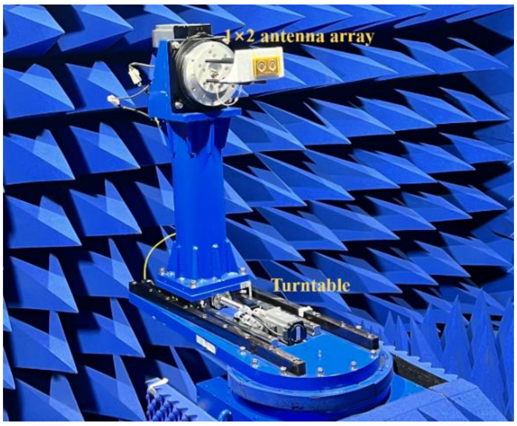

Figure 8. Measurement setup for radiation pattern.

According to Figure 9, it can be clearly seen that, before decoupling, the radiation patterns are seriously distorted because the coupled current excites the radiation of other patches, leading to poor directionality and gain reduction. This has very negative effects on the receiving power. However, the antenna's directionality and gain are greatly improved after loading the π-stub. Specifically, port 1 has a maximum measured gain of 5.5 dBi when coupled and 8.3 dBi when decoupled, showing that the π-stub is effective in decoupling the 1 × 2 RAA.

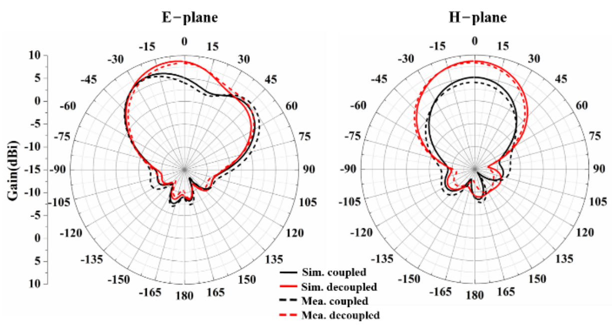

Figure 9. Simulated and measured radiation patterns of the 1 × 2 antenna arrays.

According to the comparison with other decoupled antennas shown in Table 3, the proposed π-stub decoupling network can provide good isolation at a center-to-center spacing of 0.39 λ. Moreover, the π-stub is designed to improve the receiving power of RAAs in MWPT systems, and the effectiveness is validated in Section 4.

Table 3. Comparison with other decoupled antennas.

Reference	Decoupling Structure	Frequency	Spacing	Mutual Coupling
[25]	Decoupling network	5.25 GHz	0.17 λ	−27 dB
[26]	EBG	4.95 GHz	0.36 λ	−35 dB
[27]	Decoupling network	7.5 GHz	0.5 λ	−28 dB
This work	**Decoupling network**	**5.8 GHz**	**0.39 λ**	**−27.4 dB**

3.2. The 2 × 2 RAA

RAAs for MWPT are often fabricated as rectangular arrays to expand the receiving area, so the 1 × 2 RAA was extended into a 2 × 2 RAA, as shown in Figure 10. The distance between the horizontal elements is still 0.11 λ, and the vertical distance is 0.62 λ, so the mutual coupling between port 1 and port 3 is ignorable. Due to the symmetry of the antenna, only port 1 and port 3 need to be considered. Figure 11 shows the simulated and measured S−parameter results.

It can be observed that the coupling is greatly reduced by adding the π-stub to the 2 × 2 RAA. The simulated mutual coupling reductions in adjacent elements S_{21} and S_{34} reach 13.9 and 12.7 dB, respectively, while the measured ones are 14.3 and 13.4 dB. In addition, simulated and measured radiation patterns of the coupled RAA and the decoupled RAA are shown in Figure 12. When simulated and measured, only the corresponding port is excited, and the other ports are terminated with matching loads. It can be seen that the gain after decoupling is significantly higher than that of the coupled antenna. The higher gain is more favorable for the receiving power. This will be demonstrated in the MWPT experiment.

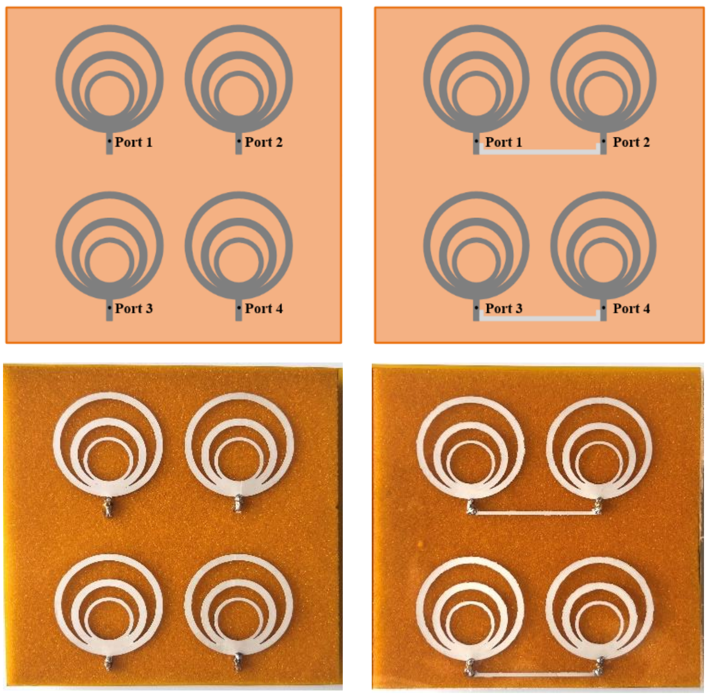

Figure 10. The geometry and prototypes of 2 × 2 RAAs.

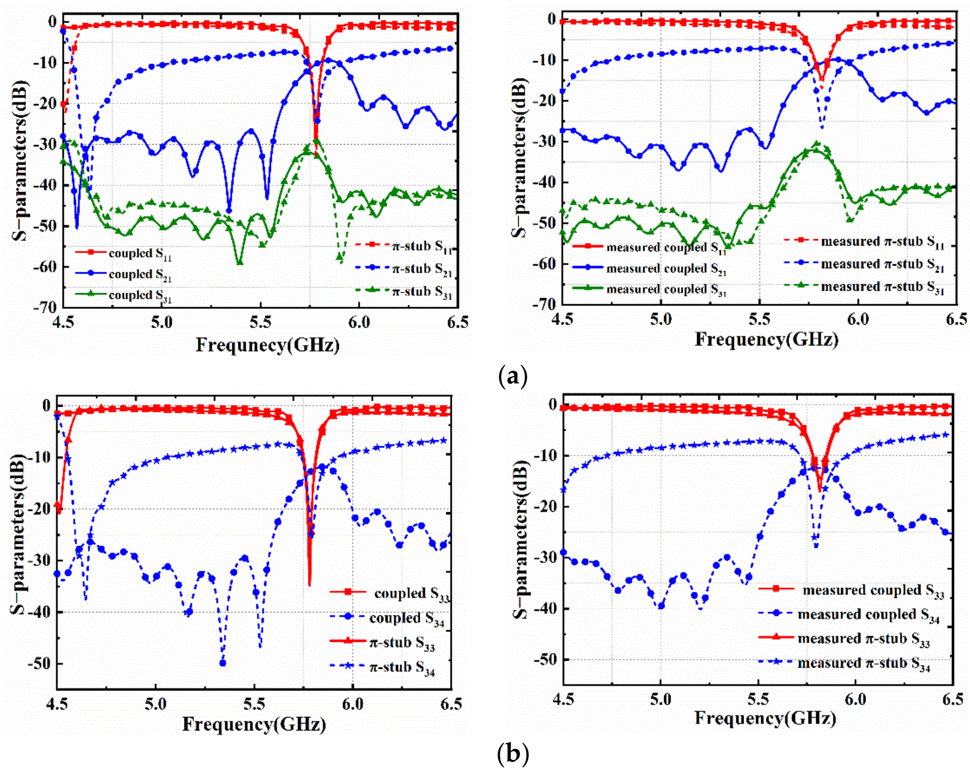

Figure 11. The simulated and measured S−parameters of 2 × 2 RAAs. (**a**) By Port 1. (**b**) By Port 3.

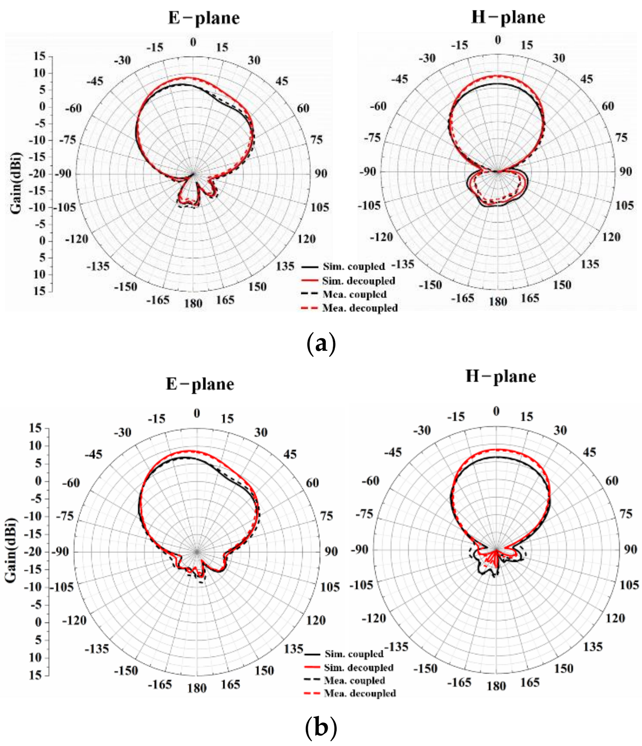

Figure 12. The simulated and measured radiation patterns of the 2 × 2 RAA. (**a**) By Port 1. (**b**) By Port 3.

4. MWPT Experiment

A miniaturized MWPT system was built to verify the value of the proposed π-stub in the MWPT application. The experimental system is shown in Figure 13.

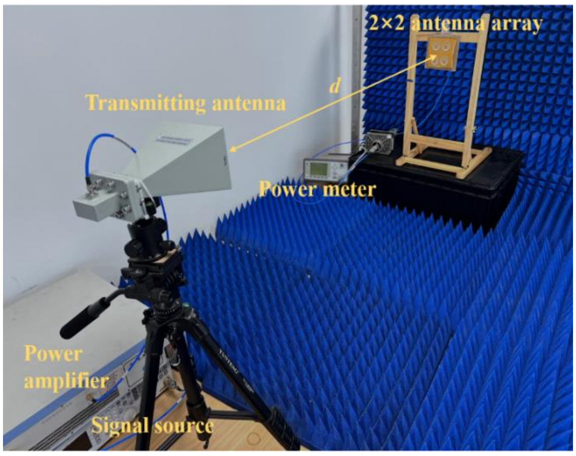

Figure 13. Miniaturized MWPT system.

In the experiment, a 5.8 GHz signal was generated by a signal source and amplified by a power amplifier. The transmitting antenna was a 5.8 GHz horn with a gain of 16 dBi. The input power of the transmitting antenna was 2 W, and the 2 × 2 RAA was placed at different positions (within the near-field range) to measure its receiving power. The geometric centers of the transmitting and receiving antennas were always aligned. The measured results are shown in Figure 14.

$$\Delta P = \frac{P_{\text{with\_}\pi-\text{stub}} - P_{\text{without\_}\pi-\text{stub}}}{P_{\text{without\_}\pi-\text{stub}}} \quad (11)$$

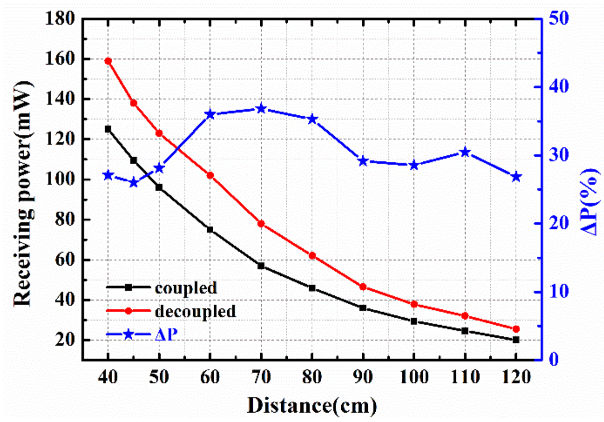

Figure 14. The receiving power of the 2 × 2 RAA.

The improvement in receiving power is denoted by ΔP, where $P_{\text{with\_}\pi-\text{stub}}$ is the measured power when the antenna array adds the proposed π-stub, and $P_{\text{without\_}\pi-\text{stub}}$ is the measured power when there is no π-stub in the antenna array. Obviously, in the range from 40 cm to 120 cm, the addition of the π-stub leads to a maximum enhancement of 36.4% of receiving power. The measured results are reduced when the RAA approaches the far-field region, which is mainly due to the power loss in free space. It is noteworthy that the improvement was maintained at more than 27% in the entire range.

5. Extended Applications

As the RAA continues to expand, too many ports will lead to high costs. So, the feed network needs to be designed to reduce the number of output ports. In this case, the proposed π-stub can be regarded as a parasitic structure combined with the feed network to improve the performance of the RAA. This can be proved by experimental results. The feed network needs to achieve good impedance matching and ensure an equal transmission phase, as shown in Figure 15. It is worth noting that, in order to combine with the feed network, π-stub 2 is rotated by 180°, and the antenna elements remain parallel to the π-stub. The feed network changes the antenna impedance matching, so the geometry of the antenna part is fine-tuned. The relevant parameters are shown in Table 4.

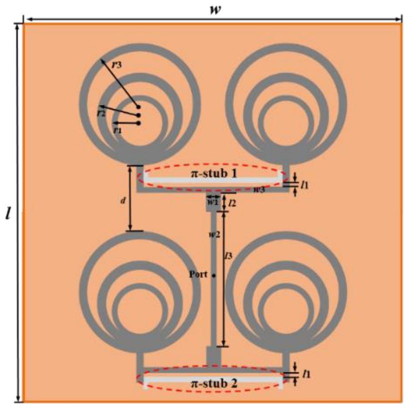

Figure 15. The geometry of RAA with feed network.

Table 4. Dimensions of the antenna array shown in Figure 15.

Parameter	Unit: mm	Parameter	Unit: mm	Parameter	Unit: mm
w	90	l	90	r_3	14.3
w_1	2.5	l_1	0.93	r_2	10
w_2	1.2	l_2	3	r_1	6.5
w_3	1	l_3	36	d	32

The prototypes were made and measured. Ant. A is the original RAA, and Ant. B has an added π-stub, as shown in Figure 16. According to the results in Figure 17, S_{11} of Ant. A and Ant. B at 5.8 GHz is −12.3 dB and −21.8 dB, respectively, indicating that Ant. B has better impedance matching. For the RAA, less power is reflected to free space.

Then, the radiation patterns were also simulated and measured, as shown in Figure 18. The results show that the radiation patterns of Ant. A and Ant. B do not produce undesirable deformation, while the gain of Ant. B is higher than that of Ant. A. The gains of Ant. A and B are 11.6 and 13 dBi, respectively. Obviously, the addition of the π-stub improves the impedance matching of the RAA and increases the gain. To further validate the results, Ant. A and Ant. B were measured using the MWPT experimental system.

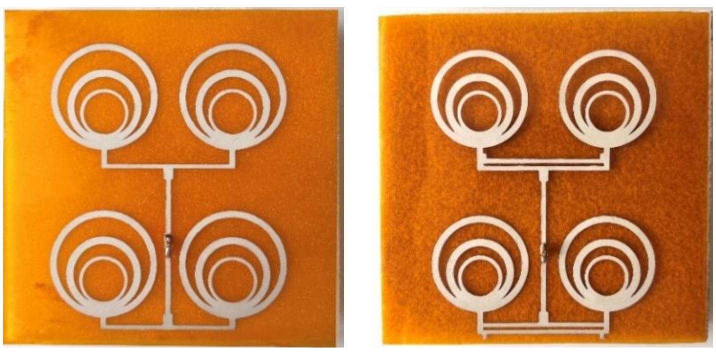

(**a**) (**b**)

Figure 16. Fabricated RAAs. (**a**) Ant. A. Without π-stub. (**b**) Ant. B. With π-stub.

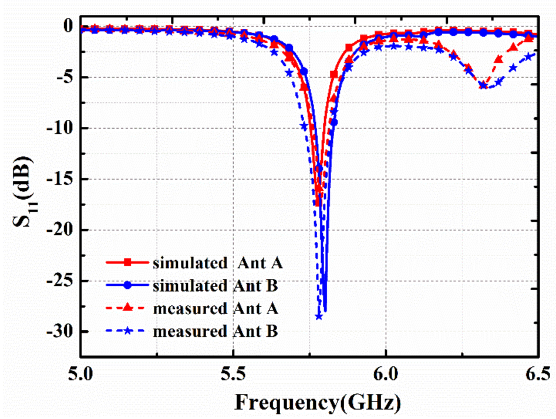

Figure 17. Simulated and measured S_{11} of Ant. A and Ant. B shown in Figure 16.

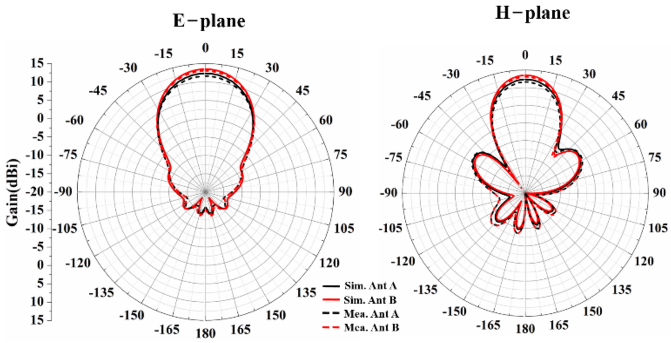

Figure 18. Simulated and measured radiation patterns of RAAs.

From the curve in Figure 19, it can be clearly seen that Ant B has a maximum of 32.3% improvement in receiving power capability. The overall results are reduced compared to Figure 14, which is caused by losses in the feed network. However, more than 17% improvement is still maintained over the entire range, verifying the scalability of the proposed π-stub.

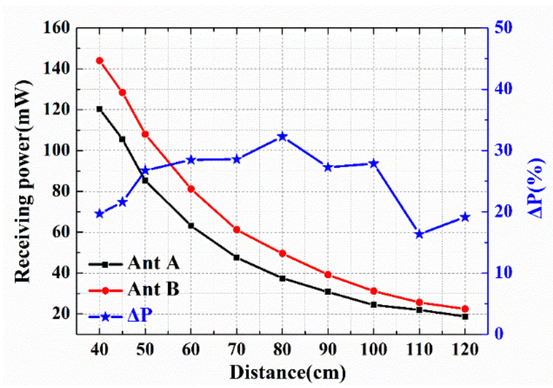

Figure 19. Comparison of the receiving power.

6. Conclusions

This study applied a decoupling network to RAAs in MWPT for the first time. The design principle and implementation form of the network were derived and combined with some specific RAAs. Compared with other decoupled structures, the proposed π-stub decoupling network can provide good isolation. Moreover, the measured results show that the proposed π-stub decoupling network can greatly improve the performance of the RAAs, including impedance matching, isolation, and gain. In addition, MWPT experiments were conducted, and the results show that the π-stub network can enhance the receiving power by up to 36.4%. Finally, the scalability of the π-stub was demonstrated by extending it to the feed network. The gain of the improved RAA is increased by 1.4 dBi with a maximum enhancement of 32.3% in receiving power. It is predicted that the proposed π-stub decoupling network will help to receive more power when the RAA is larger. Therefore, this novel decoupling network has a huge potential in high-power long-range MWPT systems.

Author Contributions: Proposed the main idea: X.L.; discussed the results and checked the whole manuscript: W.P.; contributed to the discussion of this study: H.X., H.Z. and Z.L. All authors have read and agreed to the published version of the manuscript.

Funding: This work was supported by the Chengdu-Chongqing Double-City Economic Circle construction technology innovation project under Grant KJCXZD2020001.

Data Availability Statement: The data used to support the findings of this study are included within the article.

Conflicts of Interest: The authors declare no conflict of interest.

References

1. Brown, W.C. The History of Power Transmission by Radio-Waves. *IEEE Trans. Microw. Theory Tech.* **1984**, *32*, 1230–1242. [CrossRef]
2. Wang, H.; Deng, L.; Luo, H.; Du, J.; Zhou, D.; Huang, S. Microwave Wireless Power Transfer System Based on a Frequency Reconfigurable Microstrip Patch Antenna Array. *Energies* **2021**, *14*, 415. [CrossRef]
3. Jawad, A.M.; Nordin, R.; Gharghan, S.K.; Jawad, H.M.; Ismail, M. Opportunities and Challenges for Near-Field Wireless Power Transfer: A Review. *Energies* **2017**, *10*, 1022. [CrossRef]
4. Xiao, D.; Liu, S.; Fan, L.; Zhang, H.; Peng, W. Multi-target microwave energy focusing optimization method based on genetic algorithm. *Aip Adv.* **2021**, *11*, 125004. [CrossRef]
5. Strassner, B., II; Chang, K. Microwave Power Transmission: Historical Milestones and System Components. *Proc. IEEE* **2013**, *101*, 1379–1396. [CrossRef]
6. Zhu, X.; Jin, K.; Hui, Q.; Gong, W.; Mao, D. Long-Range Wireless Microwave Power Transmission: A Review of Recent Progress. *IEEE J. Emerg. Sel. Top. Power Electron.* **2021**, *9*, 4932–4946. [CrossRef]
7. Yi, X.; Chen, Q.; Hao, S.; Chen, X. An efficient 5.8 GHz microwave wireless power transmission system. *Int. J. Rf Microw. Comput. Aided Eng.* **2022**, *32*. [CrossRef]
8. Yang, F.; Rahmat-Samii, Y. Microstrip antennas integrated with electromagnetic band-gap (EBG) structures: A low mutual coupling design for array applications. *IEEE Trans. Antennas Propag.* **2003**, *51*, 2936–2946. [CrossRef]
9. Melouki, N.; Hocini, A.; Denidni, T.A. Performance enhancement of a compact patch antenna using an optimized EBG structure. *Chin. J. Phys.* **2021**, *69*, 219–229. [CrossRef]
10. Mohsen, M.K. Using EBG to Enhance Directivity, Efficiency, and Back Lobe Reduction of a Microstrip Patch Antenna. *Prz. Elektrotechniczny* **2021**, *97*, 56–59. [CrossRef]
11. Chiu, C.-Y.; Cheng, C.-H.; Murch, R.D.; Rowell, C.R. Reduction of mutual coupling between closely-packed antenna elements. *IEEE Trans. Antennas Propag.* **2007**, *55*, 1732–1738. [CrossRef]
12. Kumar, C.; Pasha, M.I.; Guha, D. Defected Ground Structure Integrated Microstrip Array Antenna for Improved Radiation Properties. *IEEE Antennas Wirel. Propag. Lett.* **2017**, *16*, 310–312. [CrossRef]
13. Liu, R.; An, X.; Zheng, H.; Wang, M.; Gao, Z.; Li, E. Neutralization Line Decoupling Tri-Band Multiple-Input Multiple-Output Antenna Design. *IEEE Access* **2020**, *8*, 27018–27026. [CrossRef]
14. Birwal, A.; Singh, S.; Kanaujia, B.K.; Kumar, S. MIMO/Diversity Antenna with Neutralization Line for WLAN Applications. *Mapan J. Metrol. Soc. India* **2021**, *36*, 763–772. [CrossRef]
15. Li, M.; Jiang, L.; Yeung, K.L. A General and Systematic Method to Design Neutralization Lines for Isolation Enhancement in MIMO Antenna Arrays. *IEEE Trans. Veh. Technol.* **2020**, *69*, 6242–6253. [CrossRef]
16. Guo, W.-L.; Wang, G.-M.; Ji, W.-Y.; Zheng, Y.-L.; Chen, K.; Feng, Y. Broadband Spin-Decoupled Metasurface for Dual-Circularly Polarized Reflector Antenna Design. *IEEE Trans. Antennas Propag.* **2020**, *68*, 3534–3543. [CrossRef]
17. Liu, F.; Guo, J.; Zhao, L.; Huang, G.-L.; Li, Y.; Yin, Y. Dual-Band Metasurface-Based Decoupling Method for Two Closely Packed Dual-Band Antennas. *IEEE Trans. Antennas Propag.* **2020**, *68*, 552–557. [CrossRef]
18. Li, M.; Jiang, L.; Yeung, K.L. A Novel Wideband Decoupling Network for Two Antennas Based on the Wilkinson Power Divider. *IEEE Trans. Antennas Propag.* **2020**, *68*, 5082–5094. [CrossRef]
19. Mondal, P.; Dhara, D.; Harish, A.R. Enhancement of isolation between two closely spaced patch antennas using inter-digital capacitor and short-circuited stub-based band pass decoupling network. *J. Electromagn. Waves Appl.* **2022**, *36*, 669–681. [CrossRef]
20. Zou, X.-J.; Wang, G.-M.; Wang, Y.-W.; Li, H.-P. An Efficient Decoupling Network Between Feeding Points for Multielement Linear Arrays. *IEEE Trans. Antennas Propag.* **2019**, *67*, 3101–3108. [CrossRef]

21. Yi, X.; Chen, X.; Zhou, L.; Hao, S.; Zhang, B.; Duan, X. A Microwave Power Transmission Experiment Based on the Near-Field Focused Transmitter. *IEEE Antennas Wirel. Propag. Lett.* **2019**, *18*, 1105–1108. [CrossRef]
22. Qian, S.; Duan, B.; Lou, S.; Ge, C.; Wang, W. Investigation of the Performance of Antenna Array for Microwave Wireless Power Transmission Considering the Thermal Effect. *IEEE Antennas Wirel. Propag. Lett.* **2022**, *21*, 590–594. [CrossRef]
23. Chen, Q.; Chen, X.; Duan, X. Investigation on beam collection efficiency in microwave wireless power transmission. *J. Electromagn. Waves Appl.* **2018**, *32*, 1136–1151. [CrossRef]
24. Cheng, K.K.M.; Wong, F.L. A novel approach to the design and implementation of dual-band compact planar 90 degrees branch-line coupler. *IEEE Trans. Microw. Theory Tech.* **2004**, *52*, 2458–2463. [CrossRef]
25. Zhao, L.Y.; Wu, K.L. A Dual-Band Coupled Resonator Decoupling Network for Two Coupled Antennas. *IEEE Trans. Antennas Propag.* **2015**, *63*, 2843–2850. [CrossRef]
26. Liu, Y.; Yang, X.; Jia, Y.T.; Guo, Y.J. A Low Correlation and Mutual Coupling MIMO Antenna. *IEEE Access* **2019**, *7*, 127384–127392. [CrossRef]
27. Xia, R.-L.; Qu, S.-W.; Li, P.-F.; Yang, D.-Q.; Yang, S.; Nie, Z.-P. Wide-Angle Scanning Phased Array Using an Efficient Decoupling Network. *IEEE Trans. Antennas Propag.* **2015**, *63*, 5161–5165. [CrossRef]